First observation of beta-induced Alfvén eigenmode inside the edge magnetic island on the J-TEXT tokamak

J. Yang[1,2], Y. Liang[1,2,*], N.C. Wang[1], P. Shi[3], S. Zhou[1], Z.P. Chen[1], Z.H. Jiang[1], F.Y. Mao[1], J.K. Hua[1], C.K. Li[1], Q.H. Yang[1], D. Li[1], P. Drews[2], A. Knieps[2], E. Wang[2], S. Xu[2], H.M. Xiang[2], J.Q. Cai[2], J. Huang[2], Y.C. Gao[2], J.W. Liu[2], Y. Luo[2], L. Liao[2], Y.T. Yang[1], W. Xie[1], Z.Y. Chen[1], Y.H. Ding[1] and the J-TEXT team

[1] International Joint Research Laboratory of Magnetic Confinement Fusion and Plasma Physics, State Key Laboratory of Advanced Electromagnetic Engineering and Technology, School of Electrical and Electronic Engineering, Huazhong University of Science and Technology, Wuhan 430074, China
[2] Forschungszentrum Jülich GmbH, Institut für Energie- und Klimaforschung – Plasmaphysik, Partner of the Trilateral Euregio Cluster (TEC), 52425 Jülich, Germany
[3] United Kingdom Atomic Energy Authority, Culham Centre for Fusion Energy, Gulham Science Centre, Abingdon, Oxon OX14 3DB, United Kingdom

E-mail: y.liang@fz-juelich.de

Abstract. Experiments conducted on the J-TEXT tokamak have provided the first evidence that the beta-induced Alfvén eigenmode (BAE) is localized inside the isolated helical flux tube of its edge $m/n = 3/1$ magnetic island. The observations show that the BAE forms a standing wave inside the magnetic island, with its nodes located at the X- and O-points of the magnetic island. When the island is cut open by contact with the limiter plates, the BAE is found to remain inside the remnant closed island in the scrape-off layer (SOL), but its amplitude decreases as the width of the remnant island becomes smaller.

1. Introduction

Alfvén waves have been found to play a significant role in laboratory plasmas, since their interaction with energetic particles is crucial to obtaining a viable energy source in magnetically confined fusion devices such as ITER [1]. In future burning plasmas, Alfvén eigenmodes (AEs) driven by α particles [2,3] or thermal ions [4] may lead to the degradation of α confinement, preventing ignition in deuterium-tritium tokamak reactors. These instabilities can also cause enhanced energetic particle transport [5,6], leading to serious damage of reactor walls [7]. Furthermore, Alfvén eigenmodes are expected to strongly interact with thermal ions and ion temperature gradient (ITG) turbulence [8–10], which can degrade plasma confinement and be detrimental to H-mode operation in the ITER baseline scenario.

The beta-induced Alfvén eigenmode (BAE) [11], within a low-frequency gap induced by the compressional response of the plasma to shear Alfvén waves in the presence of finite pressure and curvature, was observed firstly in the DIII-D tokamak plasma with energetic ions [12]. Subsequently, BAEs accompanied by strong tearing modes were observed in ohmic plasmas without energetic particles [13–16], prompting consideration of a possible new mechanism for its excitation. Previous observations have shown that there is a critical threshold of magnetic island width for the BAE excitation [13,15], and that the BAE behaves as a pair of waves propagating in opposite directions poloidally and toroidally, forming a standing wave structure [17]. However, the detailed distribution of the BAE across the magnetic island is still not assessed. Many theoretical works were inspired to investigate the possible excitation mechanisms, such as the reversal of ion [18] and electron [19] Landau damping, and the nonlinear coupling between geodesic acoustic modes (GAMs) and magnetic islands [20]. However, due to the lack of localized measurements, the theoretical results are difficult to verify. Therefore, a complete picture of the BAE activity must be investigated.

Resonant magnetic perturbations (RMPs) play a critical role in magnetohydrodynamic stability [21]. Externally applied RMPs have shown their potential to mitigate or suppress the Alfvén modes [22,23]. In this letter, using a set of RMP coils to modify the structure of edge magnetic topology, we demonstrate for the first time that a BAE is localized inside the edge $m/n = 3/1$ magnetic island using localized measurement. Surprisingly, we find that the BAE remains inside the remnant magnetic island (the inner portion of the island not cut open by the limiter plates) located at the scrape-off layer (SOL). Radial localization is a crucial factor in understanding BAE basic characteristics. The transition from edge magnetic island to SOL magnetic island could alter the equilibrium profiles across the island,

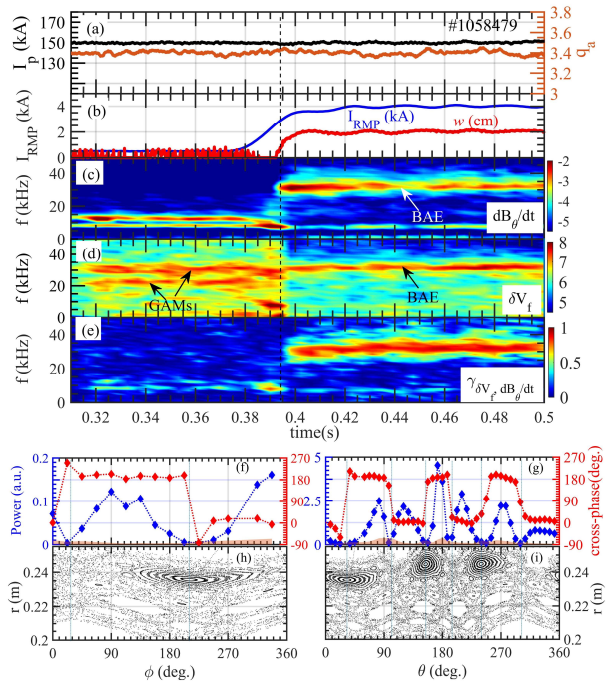

FIG. 1. Time evolution of (a) the plasma current I_p and edge safety factor q_a, (b) RMP current I_{RMP} and magnetic island width w, the spectrogram of (c) Mirnov signal dB_θ/dt, (d) floating potential fluctuation δV_f, and (e) the correlation coefficient $\gamma_{\delta V_f, dB_\theta/dt}$ between dB_θ/dt and δV_f. (e) and (f) the amplitude and cross-phase of BAE in toroidal and poloidal distributions at a given time t ~ 0.45 s. (g) and (h) the Poincaré plots at the toroidal and poloidal cross sections of dB_θ/dt measurements, respectively.

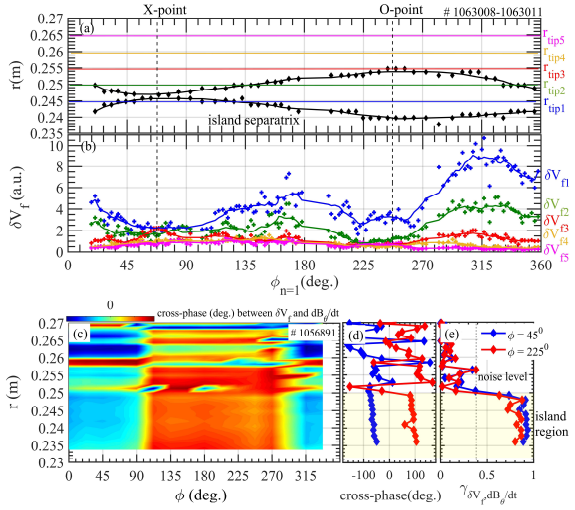

FIG. 2. (a) The vacuum calculated (black rhombus) and smooth (black line) island separatrix, with locations of the Langmuir tips presented as colored lines and (b) integrated δV_f (rhombus for measured data and curves for smooth data) in BAE frequency range as a function of RMP phase $\phi_{n=1}$. Four discharges with $q_a = 3.3$ are performed to scan the island phase over ~ 360° in the toroidal direction by changing RMP phase $\phi_{n=1}$ (1063008: $\phi_{n=1} = 198^\circ - 272^\circ$, 1063009: $\phi_{n=1} = 17^\circ - 25^\circ$ and $282^\circ - 358^\circ$, 1063010: $\phi_{n=1} = 25^\circ - 90^\circ$, 1063011: $\phi_{n=1} = 102^\circ - 178^\circ$). The cross-phase and correlation coefficients $\gamma_{\delta V_f, dB_\theta/dt}$ between δV_f and dB_θ/dt from (c) the toroidal Mirnov array and (d)-(e) two Mirnov probes at $\phi = 45^\circ$ and 225° at BAE center frequency. A combined Langmuir probe plunges through island location $\phi_{n=1} = 310^\circ$ in the discharge #1056891 with $q_a = 3.4$. The yellow shadow indicates the island region.

which will provide consideration for what excites or sustains BAEs. Therefore, these findings offer valuable insights into the BAE excitation mechanism and provide a basis for further theoretical investigations and predictions.

2. Experimental setup

The presented observations were obtained at the J-TEXT facility. J-TEXT is a medium-size tokamak operated at a major radius R = 1.05 m and minor radius a = 0.25-0.29 m with a circular cross-section. In this experiment, the target hydrogen plasma was performed in an Ohmic discharge with high reproducibility. The radial position of the $q = 3$ rational surface can be shifted by turning the plasma current I_p. These plasmas had a toroidal field of $B_t = 1.4\,T$, the center line-averaged density of $n_e \sim 1.5 \times 10^{19}\ m^{-3}$. The limiters located at the low-field-side (LFS) and the bottom-side were installed at the poloidal cross section with a toroidal angle of $\phi = 337.5^\circ$. Both of them were positioned at the minor radii of 0.255 m, as the main limiters. The RMP system consists of 24 in-vessel saddle coils, including 12 single-turn coils and 12 double-turn oils

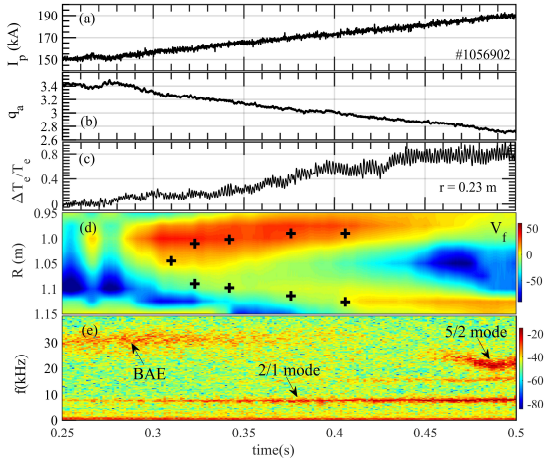

FIG. 3. Time evolution of (a) plasma toroidal current I_p, (b) edge safety factor q_a, (c) the variations of normalized edge electron temperature $\Delta T_e/T_e (= (T_e - T_e(t = 0.25\,s))/T_e(t = 0.25\,s))$ at r = 0.23 m at the HFS, (d) the floating potential V_f distribution on the bottom limiter and the calculated strike points (+) and (e) the spectrogram of $\partial B_\theta/\partial t$ from a toroidal Mirnov probe.

[24]. In this letter, an RMP in m/n = 3/1 configuration is applied to produce an edge magnetic island at the $q = 3$ resonant surface. m and n refer to the poloidal and toroidal mode numbers. The Mirnov signals dB_θ/dt are measured by the toroidal Mirnov array (poloidal angle $\theta = -45^\circ$) and the poloidal Mirnov array (toroidal angle $\phi = 56.25^\circ$) [25]. The manipulator capable of carrying different Langmuir probes are installed on the top window ($\phi = 292.5^\circ$, $\theta = 90^\circ$), which can provide the local floating potential V_f, electron temperature T_e and density n_e, radial electric field $E_r = -dV_f/dr - 2.5dT_e/dr$ and electron pressure $P_e = T_e n_e$ [26].

3. Experimental results

3.1. Observation of BAE inside edge magnetic island

Figure 1(a)-(e) show an overview of BAE observations from discharge #1058479 with $q_a = 3.4$. The time traces are the plasma current I_P, edge safety factor q_a, the current of one of the RMP coils I_{RMP}, the magnetic island width w measured by a set of saddle loops [27], the spectrogram of Mirnov signal dB_θ/dt, V_f fluctuation δV_f at r = 0.245 m and the correlation coefficient $\gamma_{\delta V_f, dB_\theta/dt}$ between dB_θ/dt and δV_f. A 3/1 magnetic island is excited at t ~ 0.395 s and subsequently saturates with w ~ 2 cm, as shown in Fig. 1(b). The width of the 3/1 magnetic island has also been identified by the flattening of the edge P_e profile [28] measured by a combined Langmuir probe, as shown in Fig. 4 (d). Before RMP penetration, two electrostatic GAMs with frequencies $f \approx$ 21 kHz and 30 kHz are observed in δV_f. After RMP penetration, these two GAMs are suppressed and a BAE with $f \approx$ 31 kHz is visible in dB_θ/dt and δV_f synchronically. The observed BAE frequency has been demonstrated to lie within the BAE gap in the continuous spectrum calculated by the NOVA-K code [29]. It should be noted that NOVA-K code is based on the nested magnetic flux surfaces. Additionally, $T_e \approx 32\ eV$ is observed inside the edge closed island from Fig. 4(b). Based on the theoretical frequency $f_{BAE}^{theo} = \frac{1}{2\pi R}[\frac{T_e}{m_i}(\frac{7}{2}\frac{T_i}{T_e} + 2)]^{1/2}$ [30] and observation of $T_i \approx (2-3)T_e$ at low density of J-TEXT [31], the BAE frequency is predicted to be 27-32 kHz when taking the Doppler shift of 1.7 kHz into account, covering the observed frequency 31 kHz. The Fourier transform is use to extract the intensity and mode-number of BAE in dB_θ/dt. The auto-power of dB_θ/dt in BAE frequency range (30~35 kHz) and the cross-phase between dB_θ/dt at the BAE center frequency (~31 kHz) are shown in Fig. 1(f) and (g). A reference channel near the maximum mode intensity is selected for the cross-phase. The BAE has m/n = 3/1 mode numbers and exhibits a standing-wave structure. The standing wave nodes, identified by an 180° flip of the cross-phase, are located at

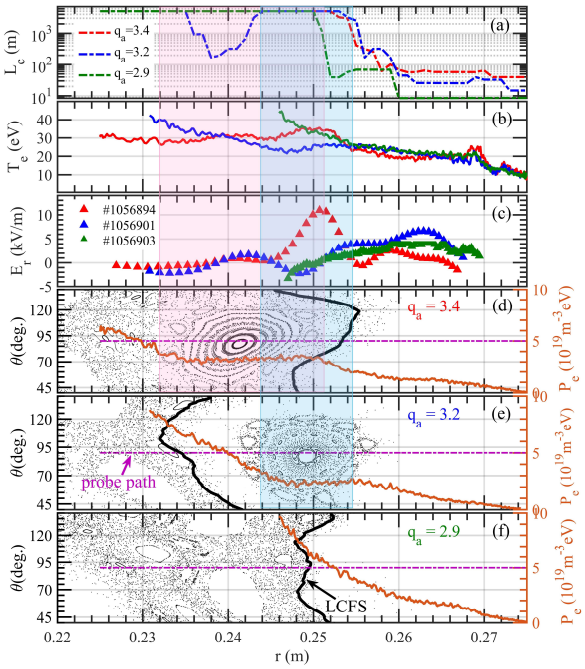

FIG. 4. Radial profiles for three cases with $q_a = 3.4$, 3.2 and 2.9 of (a) calculated connection length L_c along the Langmuir probe path, (b) measured electron temperature T_e and (c) radial electric field E_r. (d)-(f) The corresponding Poincaré plots at the poloidal cross section of the Langmuir probe, overlaid with electron pressure P_e. Purple dotted lines indicate the probe paths, and thick black lines represent the estimated LCFS. The pink and blue shadows indicate the island regions.

the O- and X-points of the m/n = 3/1 magnetic island as shown in the Poincaré plots at the cross sections of dB_θ/dt measurements (Fig. 1(h) and (i)). Here, the Poincaré plot is calculated using a vacuum field line tracing code, which is the equilibrium field from the EFIT code [32] plus the vacuum perturbation fields from the RMP coils. These characteristics conform to the feature of BAE on J-TEXT [29]. It should be noted that in the tracing code, the rotation screening effect is ignored, which has greater limitation on the RMP penetration at the core while has less limitation at the edge.

To clarify the spatial structure of the BAE precisely, four discharges #1063008-1063011 with $q_a = 3.3$ were performed to scan the island phase over 360° in the toroidal direction by changing the RMP phase $\phi_{n=1}$ (~90° per discharge). A 5-tip radial Langmuir probe array is positioned at the plasma edge to provide δV_{f1}, δV_{f2}, δV_{f3}, δV_{f4} and δV_{f5} during the phase scanning. The positions of tips 1-5 are indicated by the different colored lines in Fig. 2(a). An m/n = 3/1 magnetic island with a width of ~ 1.5 cm appears at $r \approx$ 0.246 m, as indicated by the vacuum calculated separatrix (black rhombus) of the island at the location of V_f measurement shown in Fig. 2(a). Tips 1 and

2 are located inside the magnetic island, and tips 3, 4 and 5 are on the outer side. Fig. 2(b) presents the integrated δV_f in the BAE frequency range. δV_{f3}, δV_{f4} and δV_{f5} keep low levels over $\phi_{n=1}$. In contrast, δV_{f1} and δV_{f2} exhibit strong signals in the space between O- ($\phi_{n=1} = 250^{\circ}$) and X-point ($\phi_{n=1} = 70^{\circ}$), consistent with the standing wave feature of BAE. Additionally, δV_{f1} is larger than δV_{f2}, and tip 1 is positioned radially closer to the island center. Therefore, we can conclude that BAE is located inside the magnetic island and stronger between the X- and O-point of the magnetic island. This result can also be demonstrated by the high correlation coefficient $\gamma_{\delta V_f, dB_\theta/dt}$ between δV_f and dB_θ/dt at toroidal position $\phi = 45^{\circ}$ and 225° at BAE center frequency inside the island (yellow shadow region), as shown in Fig. 2(e). Here δV_f is from a combined Langmuir probe plunging through the island position $\phi_{n=1} = 310^{\circ}$ in the discharge #1056891 with $q_a = 3.4$. As shown by the cross-phases between δV_f and dB_θ/dt in Fig. 2(c) and (d), the phase of BAE is reversed 180 degrees toroidally at the nodes but unchanged radially.

3.2. Observation of BAE inside remnant magnetic island

Furthermore, the dynamics of BAE during the opening of the edge magnetic island were investigated. As shown in Fig. 3 (a) and (b), I_p increases from 150 kA to 195 kA in discharge #1056902, leading to a decrease in q_a from 3.4 to 2.7. In figure 3 (d), the floating potential V_f measured by the Langmuir probes mounted on the bottom limiter [33] are shown, together with the evolution of the calculated strike points (black crosses). The strike points are formed by the intersection of the edge magnetic island with the bottom limiter target plate, and calculated by the vacuum field line tracing code. By tracing the field lines from the bottom limiter into the SOL or core plasma, the location of the strike points can be determined from the peak of the minimum normalized poloidal magnetic flux ψ_{min} distribution, so called the penetration depth [34]. At t ~ 0.31 s (q_a~3.25), the edge 3/1 magnetic island begins to touch the bottom limiter, transitioning to an open magnetic island. As I_p increases further, two splitting strike points are generated on the bottom limiter and the distance between them gradually increases. The locations of the calculated strike points follow the trend of the changing paths of the maximum and minimum values of V_f. The strong dependence of V_f on the strike points has been reported in DIII-D and MAST [35–37]. The V_f observations are only qualitative since the distribution of V_f is complicated when taking the plasma transport, such as finite orbit effect and drift effects, etc.

During this process, it's very interesting to observe that the BAE gradually disappear at an almost constant frequency $f \approx 31$ kHz. This result can be repeatable, except for some discharges in which the BAE frequency slightly drops as q_a decreases. Besides, the variations of the normalized edge electron temperature $\Delta T_e/T_e (= (T_e - T_e(t = 0.25\,s))/\,T_e(t = 0.25\,s))$ at r = 0.23 m of the high-field-side (HFS) measured by electron cyclotron emission (ECE) is gradually increased, which is consistent with the increase of T_e at r < 0.24 m in figure 4 (b). This increase may be the combined effects of the increase in I_p (input Ohmic power) and inward shift in the location of T_e measurement relative to the last closed flux surface (LCFS).

To illustrate the dynamics of the edge magnetic topology during the opening of the edge magnetic island, a series of discharges (#1056894, #1056901, #1056903) with different q_a (3.4, 3.2 and 2.9) were performed. Fig. 4(d)-(f) present three Poincaré plots calculated with plasma parameters from the three discharges, overlaid with plasma pressure P_e profiles. For $q_a = 3.4$, an edge closed 3/1 island with a width of ~2 cm is located at r ≈ 0.242 m (pink shadow region), very close to the LCFS. Here, the LCFS is represented by a thick black line and estimated as the radial position where the connection length L_c reaches infinity. The flat region of pressure P_e profile is consistent with the radial region where the 3/1 island is located in the Poincaré plot, confirming the accuracy of the calculated edge magnetic island. As q_a decreases to 3.2, the island is pushed outwards to intersect the local limiter, resulting in a closed remnant magnetic island of ~1.0 cm (blue shadow region) located in the SOL between the LCFS and the limiter. In this case, the edge topology becomes very similar to the island divertor configuration in W7-X [38] and LHD [39]. It should be pointed out that in order to illustrate the smaller distance between the $q = 3$ resonant surface and limiter targets, the fixed minor radius a = 0.255 m is used in the calculation of q_a, ignoring the fact that the minor radius a becomes smaller after the magnetic island touches the targets. As q_a continues to decrease, the limiter

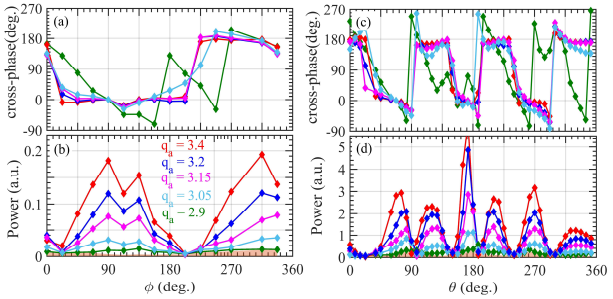

FIG. 5. Cross-phase analysis of dB_θ/dt in toroidal and poloidal distributions for five q_a slots of Fig. 3. (a) and (c) cross-phase at BAE center frequency, (b) and (d) auto-power of dB_θ/dt in BAE frequency range. The pink shadow indicates the noise level of dB_θ/dt.

cuts the island progressively, causing a shrinking width of the remnant island. For $q_a = 2.9$, the island is fully cut by the limiter, and there is no remnant island structure present in the SOL. As q_a decreases from 3.4 to 3.2, the flat P_e profile is shifted outward and becomes narrow in width from ~1.7 cm to ~1.0 cm, providing powerful evidence for the modifications of the magnetic islands.

The changes in the structure of edge magnetic topology are also manifested in the connection length L_c along the Langmuir probe path (Fig. 4(a)) and the edge E_r profile (Fig. 4(c)). For $q_a = 3.2$, L_c is infinite inside the remnant island and drops to a finite value at the gap between the remnant island and LCFS due to the fact that the magnetic field lines of this gap are connected to the limiters. E_r develops a negative well inside the remnant island and towards positive values at the gap, indicating that electrons are well confined at the closed region but lost faster than ions along the open magnetic field lines [40].

Figure 5 plots the distributions of cross-phases and intensity of BAEs for five q_a slots of Fig. 3. BAE remains inside the remnant island ($q_a = 3.2$, 3.15 and 3.05), but its intensity decreases as the width of the remnant island becomes smaller. The discharge #1056901 with a fixed $q_a = 3.2$ indicates that BAE can be excited in the present of a remnant magnetic island. For $q_a = 2.9$, the cross-phase no longer exhibits the standing wave structure, and the BAE intensity is comparable to the noise level (pink shadow), indicating that the BAE entirely disappears in the absence of a remnant island.

4. Discussion and conclusion

Unlike the results from other devices, there is no obvious link between the BAE frequency and the remnant magnetic island's width. As the edge topology transitions from an edge island to a remnant island, T_e inside the island is decreased from 32 eV to 25 eV (Fig. 4(b)), while the ratio of the ion-to-electron temperature T_i/T_e is observed to increase from the plasma edge to SOL on J-TEXT due to the higher thermally decoupled in the deeper SOL [31]. From the theoretical predicted frequency $f_{BAE}^{theo} = \frac{1}{2\pi R}[\frac{T_e}{m_i}(\frac{7}{2}\frac{T_i}{T_e} + 2)]^{1/2}$, the BAE frequency is expected to have no or a moderate change in the experiments. In additional, the results share some similarities with previous results, i.e., that the strength of BAE decreases as the island size becomes smaller. But the remnant magnetic island is emphasized here, which is located at the SOL and surrounded by the opened magnetic field lines connecting to the limiters. The particle and heat fluxes, which reach these opened flux tubes, steam toward the limiter plates and miss the isolated remnant island region [41], resulting in a reduction in temperature T_e, density n_e and pressure P_e inside the remnant island. Despite with a reduced beta (ratio of thermal energy to magnetic energy) and a flat pressure profile, the BAE is still present. It's worth noting that inside the remnant island, non-flat distributions of T_e and n_e as well as a negative E_r well (Fig. 4(b) and (c)) are presented.

The radial structure of the shear Alfvén wave continuous spectrum is calculated in the presence of a magnetic island [42–44]. One shear Alfvén continuum is found at the O-point of the magnetic island, and another shear Alfvén continuum is found to be positioned at the separatrix flux surface of the magnetic island. Neither of these two continuums is perfect agreement with the BAE observed in this experiment. Furthermore, BAE is generally damped by the thermal ion Landau damping, therefore, BAE is expected to strongly damp when the pressure value is decreased inside the remnant island. This may be one of the reasons why the BAE intensity gradually decreases during the opening of the edge magnetic island.

In conclusion, the experimental data from the J-TEXT tokamak identify for the first time the radial localization of BAE inside the edge m/n = 3/1 magnetic island by local measurement with Langmuir probes. The maximal amplitude of BAE is found to occur between the X- and O-points of the magnetic island, and the phase of BAE is unchanged in the radial direction. Moreover, during the opening of the edge magnetic island, the BAE is observed to remain inside the remnant closed island, but its intensity decreases as the width of the remnant island becomes smaller. These observations are of significant importance in comprehending the drive and damping mechanisms of BAE, and predicting Alfvénic activity and its nonlinear consequences in the future devices, and also raises an open question of what is the role of the magnetic island structure in exciting or sustaining the BAE. More theoretical and simulation studies may be necessary to clarify the underlying mechanisms.

Acknowledgements

This work is supported by the National MCF Energy R&D Program of China (Grant No. 2018YFE0309100), the National Key R&D Program of China (Grant No.2017YFE0302000), the EPSRC Energy Program (grant No. EP/W006839/1) and the National Natural Science Foundation of China (Grant No. 51821005).

References

[1] M. Shimada et al., Progress in the ITER Physics Basis Chapter 1: Overview and summary 2007 Nucl. Fusion 47 S1.

[2] S. E. Sharapov et al., 2002 Phys. Plasmas 9, 2027.

[3] R. Nazikian et al., 1997 Phys. Rev. Lett. 78, 2976.

[4] R. Nazikian et al., 2006 Phys. Rev. Lett. 96, 105006.

[5] C. S. Collins et al., 2016 Phys. Rev. Lett. 116, 095001.
[6] W. W. Heidbrink et al., 2007 Phys. Rev. Lett. 99, 245002.
[7] H. H. Duong, W. W. Heidbrink, E. J. Strait, T. W. Petrie, R. Lee, R. A. Moyer and J. G. Watkins, 1993 Nucl. Fusion 33, 749.
[8] H. S. Zhang, Z. Lin, and I. Holod, 2012 Phys. Rev. Lett. 109, 025001.
[9] P. Liu, X. Wei, Z. Lin, G. Brochard, G. J. Choi, W. W.Heidbrink, J. H. Nicolau, and G. R. McKee, 2022 Phys. Rev. Lett. 128, 185001.
[10] A. Biancalani et al., 2021 Plasma Phys. Controlled Fusion 63, 065009.
[11] A. D. Turnbull, E. J. Strait, W. W. Heidbrink, M. S. Chu, H. H. Duong, J. M. Greene, L. L. Lao, T. S.Taylor, and S. J. Thompson, 1993 Phys. Fluids B 5, 2546.
[12] W. W. Heidbrink, E. J. Strait, M. S. Chu, and A. D. Turnbull, 1993 Phys. Rev. Lett. 71, 855.
[13] P. Buratti, P. Smeulders, F. Zonca, S. Annibaldi, M. D. Benedetti, H. Kroegler, G. Regnoli, O. Tudisco, and the FTU-team, 2005 Nucl. Fusion 45, 1446.
[14] P. Buratti, O. Zimmermann, M. De Benedetti, Y. Liang, H. Koslowski, G. Regnoli, O. Smeulders, and F. Zonca, 2005 in Proc. 32nd EPS Conf. on Plasma Physics, Vol. 29, https://www.afs.enea.it/zonca/references/conference/buratti_eps05.pdf.
[15] G. Pucella et al., 2022 Plasma Phys. Control. Fusion 64 045023.
[16] L. Piron et al., 2023 Fusion Eng. Des. 195, 113957.
[17] W. Chen et al., 2010 Phys. Rev. Lett. 105, 185004.
[18] V. Marchenko and S. Reznik, 2009 Nucl. Fusion 49, 022002.
[19] V. Marchenko, A. Panwar, S. Reznik, and C. Ryu, 2016 Nucl. Fusion 56, 106021.
[20] H. Cai, B. Gao, M. Xu, A. Liu, and D. Kong, 2021 Nucl. Fusion 61, 036029.
[21] Y. Liang et al., 2007 Phys. Rev. Lett. 98, 265004.
[22] A. Bortolon, W. W. Heidbrink, G. J. Kramer, J.-K. Park, E. D. Fredrickson, J. D. Lore, and M. Podestà, 2013 Phys. Rev. Lett. 110, 265008.
[23] G. J. Kramer et al., 2016 Plasma Phys. Controlled Fusion 58, 085003.
[24] Y. Liang et al., 2019 Nucl. Fusion 59, 112016.
[25] D. Guo et al., 2017 Rev. Sci. Instrum. 88 123502.
[26] P. C. Stangeby and G. M. McCracken, 1990 Nucl. Fusion 30 1225–379.
[27] R. Fitzpatrick, 1993 Nucl. Fusion 33 1049.
[28] C. C. Hegna and J. D. Callen, 1992 Phys. Fluids B 4, 4072.
[29] L. Liu et al., 2019 Nucl. Fusion 59, 126022.
[30] F. Zonca, L. Chen, and R. A Santoro, 1996 Plasma Phys. Controlled Fusion 38, 2011.
[31] H. Liu et al., 2021 Plasma Phys. Controlled Fusion 63, 075004.
[32] M. Fitzgerald, L. C. Appel and M. J. Hole, 2013 Nucl. Fusion 53 113040.
[33] J. Yang et al., 2019 Plasma Sci. Technol. 21 105105.
[34] D. M. Harting et al., 2012 Nucl. Fusion 52 054009.
[35] J. G. Watkins et al., 2009 J. Nucl. Mater. 390–391 839–42.
[36] D. M. Orlov et al., 2014 Nucl. Fusion 54 093008.
[37] P. Cahyna et al., 2013 J. Nucl. Mater. 438 S326–9.
[38] E. Strumberger, 1996 Nucl. Fusion 36, 891.
[39] A. Komori et al., 2005 Nucl. Fusion 45, 837.
[40] Y. Suzuki et al., 2016 Nucl. Fusion 56, 092002.
[41] M. W. Jakubowski et al., 2006 Phys. Rev. Lett. 96, 035004.
[42] A. Biancalani, L. Chen, F. Pegoraro and F. Zonca, 2010 Phys. Rev. Lett. 105, 095002.
[43] A. Biancalani, L. Chen, F. Pegoraro and F. Zonca, 2011 Plasma Phys. Control. Fusion 53, 025009.
[44] C. R. Cook and C. C. Hegna 2015 Phys. Plasmas 22 042517.